



Non-Single Viewpoint Catadioptric Cameras: Geometry and Analysis

RAHUL SWAMINATHAN, MICHAEL D. GROSSBERG AND SHREE K. NAYAR

Department of Computer Science, Columbia University, New York, NY 10027, USA

srahul@cs.columbia.edu

mdog@cs.columbia.edu

nayar@cs.columbia.edu

Received January 8, 2002; Revised August 11, 2003; Accepted February 25, 2005

Abstract. Conventional vision systems and algorithms assume the imaging system to have a single viewpoint. However, these imaging systems need not always maintain a single viewpoint. For instance, an incorrectly aligned catadioptric system could cause non-single viewpoints. Moreover, a lot of flexibility in imaging system design can be achieved by relaxing the need for imaging systems to have a single viewpoint. Thus, imaging systems with non-single viewpoints can be designed for specific imaging tasks, or image characteristics such as field of view and resolution. The viewpoint locus of such imaging systems is called a caustic.

In this paper, we present an in-depth analysis of caustics of catadioptric cameras with conic reflectors. We use a simple parametric model for both, the reflector and the imaging system, to derive an analytic solution for the caustic surface. This model completely describes the imaging system and provides a map from pixels in the image to their corresponding viewpoints and viewing direction. We use the model to analyze the imaging system's properties such as field of view, resolution and other geometric properties of the caustic itself. In addition, we present a simple technique to calibrate the class of conic catadioptric cameras and estimate their caustics from known camera motion. The analysis and results we present in this paper are general and can be applied to any catadioptric imaging system whose reflector has a parametric form.

Keywords: catadioptric system, conic section, non-single viewpoint, caustics, viewpoint surface, self-calibration, sensor resolution

1. Introduction

Traditionally, imaging systems have been designed to maintain a single viewpoint. In other words, all the rays of light entering the imaging system intersect at a single point, called the effective viewpoint. This single viewpoint model is extensively used in many vision algorithms. Most dioptric (lens-based) imaging systems are assumed to maintain a single viewpoint. The perspective lens based camera is a special type of a single viewpoint imaging system. Note that, imaging systems with a single viewpoint are not limited to dioptric systems alone. Catadioptric (combination of lens and

mirrors) imaging systems have also been designed with the aim of maintaining a single effective viewpoint.

Single viewpoint catadioptric cameras include multi-sensor planar mirror systems for panoramic imaging (Nalwa, 1996) as well as for stereo applications (Gluckman and Nayar, 1999). Curved mirrors have also been used in the past. For instance, hyperbolic (Rees, 1970; Yamazawa et al., 1993) and parabolic (Nayar, 1997; Baker and Nayar, 1998; Peri and Nayar, 1997) mirrors have already been shown to produce single viewpoint catadioptric sensors. These systems consist of a perspective or telecentric¹ lens and a reflector. The pinhole (entrance pupil) of the lens

is positioned at one of the focal points of the reflector, making the other focal point the effective viewpoint. However, such systems require precise assembly of the imaging components, failing which the viewpoint deviates from a single point.

Cameras need not always obey the single viewpoint constraint. Relaxing this constraint, gives greater flexibility in designing imaging systems. Thus, if we allow for deviations from a single viewpoint we can trade-off image characteristics such as field of view and spatial resolution. Catadioptric cameras that do not maintain a single view point include the spherical and conical reflector based designs (Hong et al., 1990; Yagi and Yachida, 1991; Yagi et al., 1994; Bogner, 1995; Murphy, 1997; Charles et al., 1987; Bolles et al., 1997; Derrien and Konolige, 2000). Chahl and Srinivasan (1997) developed a specially shaped reflector in so that the visible solid angle at each pixel is the same. Hicks and Bajcsy (2000) developed a wide angle perspective projection camera system also using specially shaped reflectors. In Nayar and Karmarkar (2000), a conical mirror system was proposed to capture a high resolution 360×360 degree stereo panorama. In Hicks (2002), Srinivasan (2003), a new class of imaging systems were presented that directly acquire a cylindrical panorama. None of these imaging systems maintain a single viewpoint. However, the images acquired by such imaging systems were processed ignoring non-single viewpoint effects. Ideally, the imaging geometry must be understood in order to correctly process the acquired images.

When an imaging system does not maintain a single viewpoint, a locus of viewpoints in three dimensions is formed, called a caustic (Born and Wolf, 1965). The caustic is defined as a singularity in the space of the scene rays. The caustic represents the envelope of all incoming scene rays which are eventually imaged. Each pixel in the image maps to a point on the caustic surface. Also, every point on the caustic maps to a unique light ray from the scene which eventually gets imaged. Thus, caustics completely describe the geometry of an imaging system.

Certain applications demand the imaging system to have a specific viewpoint surface. In such cases, one can imagine designing specific imaging systems keeping this desired viewpoint locus in mind. For instance, Baker and Nayar (1998) the caustic was restricted to a single point. Peleg et al. (2000), a stereo sensor was designed by constraining the caustic of the camera to be a circle. Also, mosaics constructed under camera mo-

tion using perspective or non-single viewpoint cameras have been used for stereo reconstruction (Pajdla, 2002; Seitz, 2001). Non-single viewpoint sensors have also been designed to provide specific imaging geometries, such as near-perspective projection for a specific plane in the scene (Hicks and Bajcsy, 2000), specific resolution distributions (Hicks and Perline, 2002; Gaspar et al., 2002; Gachter et al., 2001), amongst other applications (Weinshall et al., 2002; Pajdla, 2001, 2002).

This paper analyzes caustics of conic catadioptric systems. By this we mean that the profile of the mirror is a conic section. Conic reflector based cameras are widely used in vision as well as in astronomical applications. Also, most surfaces can be locally approximated by quadrics. It is therefore important to analyze the viewpoint loci of such imaging systems. In particular, we raise the following questions:

- What happens to the viewpoint locus when a system deviates from a single viewpoint? Note that in spite of using a perspective lens, the catadioptric system need not have a single viewpoint. Instead, the viewpoint locus is described by a caustic surface.
- How does this viewpoint surface affect optical resolution characteristics. Specifically, how does the mirror shape, and relative positioning of the lens elements affect resolution?
- Finally, given a viewpoint model, is there a simple way to calibrate such non-single viewpoint systems? Note that in spite of using a perspective lens and reflector, the system as a whole need not maintain a single viewpoint. Calibration entails finding the map between every pixel in the image and its corresponding viewpoint.

We begin by deriving the caustic surface for a family of conic catadioptric systems. By careful parameterization of the reflector profile, we present a simple derivation of the viewpoint locus as a three parameter family of curves. These caustic surfaces are then analyzed for their effects on resolution, field of view, and geometric singularities. In our analysis we consider the principal rays passing through the entrance pupil of the camera lens to describe the geometry of the imaging system. Secondary effects such as blurring² (due to bundles of rays) do not interfere with the geometric analysis we present. Finally, we present a simple self-calibration technique to estimate the parameters that describe the caustic surface numerically for a catadioptric camera using known camera motion. Although every pixel has

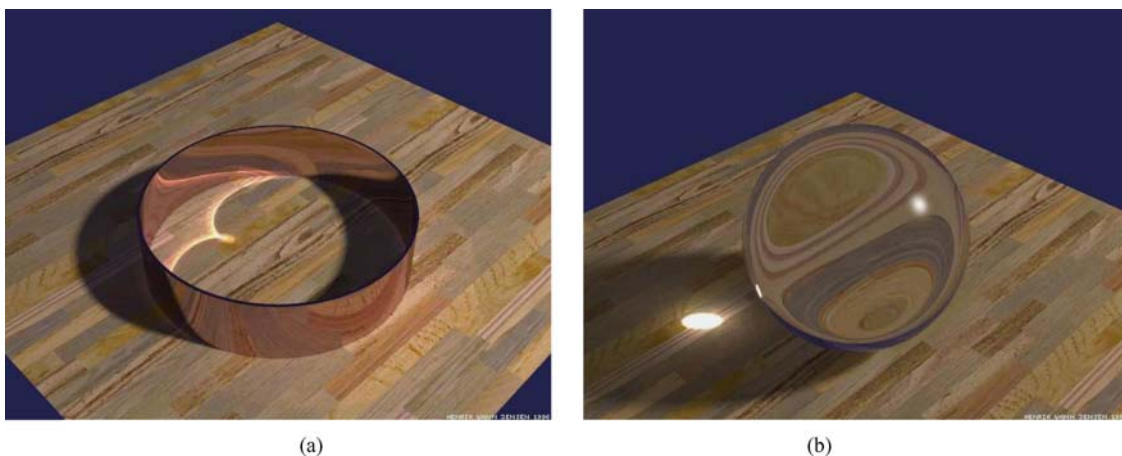


Figure 1. The caustics formed due to light (a) reflecting off the inside of a metal ring and (b) refracting through a spherical lens. Bright patterns of light on the table illustrate a section of the caustic surface formed. These bright patterns are due to the close bunching together of light rays near the caustic's surface. Adapted from Jensen (1996).

an unique viewpoint, calibration of such non-single viewpoint sensors is reduced to estimating only a few parameters.

2. Caustics: Loci of Viewpoints

When a light ray interacts with either a reflective or refractive interface, it may bend and thus alter its path. These reflected or refracted rays often form an envelope, called the caustic surface (Hamilton, 1828; Born and Wolf, 1965). A caustic can be defined as a locus of singularities of these ray (Arnold, 1978; Burkhard and Shealy, 1973). Caustics formed by reflecting elements are called *catacaustics* and those by refractive elements are called *diacaustics*. Figure 1 illustrates caustics formed by (a) reflection by a metal ring and (b) refraction through a transparent sphere. Near the caustic, the rays of light bunch up together, thus forming bright patterns as seen in the images. Henceforth, we use the term caustic to mean both the catacaustic as well as the diacaustic.

With respect to imaging devices, caustics represent their loci of viewpoints. The single viewpoint is a degenerate case of a point caustic. Each point on the caustic surface represents the three-dimensional position of a viewpoint and its viewing direction. Thus, the caustic completely describes the geometry of the camera. One can represent compound imaging systems consisting of multiple imaging components, such as lenses and reflectors, by simply their effective caus-

tics (see also (Swaminathan et al., 2001; Grossberg and Nayar, 2001)).

2.1. Computing the Caustic

We now study caustics of catadioptric imaging systems consisting of a perspective or telecentric lens and a single reflector whose profile is a conic section. Although we use the perspective or telecentric (orthographic projection) lens, the imaging system as a whole (including the reflector) need not maintain a single viewpoint.

In analyzing these imaging systems, we follow the framework of geometric optics. Therefore, for every pixel we only consider the chief or principal ray associated with it. In reality, every pixel is associated with a bundle of rays from the scene. These rays are needed to analyze secondary effects such as blurring which are, however, beyond the scope of this paper.

Many techniques have been proposed to derive the caustics of reflecting and refractive systems including the ones based on a local conic approximations (Bruce et al., 1981) and the Jacobian method (Burkhard and Shealy, 1973). In (Bruce et al., 1981), the central idea lies in fact that for conic sections the light rays emanating from one of the focal points all meet at the second focal point. To estimate the caustic point corresponding to a point on an arbitrary curve, we first approximate the curve locally by a conic section such that one of the foci lies at the entrance pupil of the lens. Thus, the second focal point (derived analytically) is the corresponding point on the caustic curve. However,

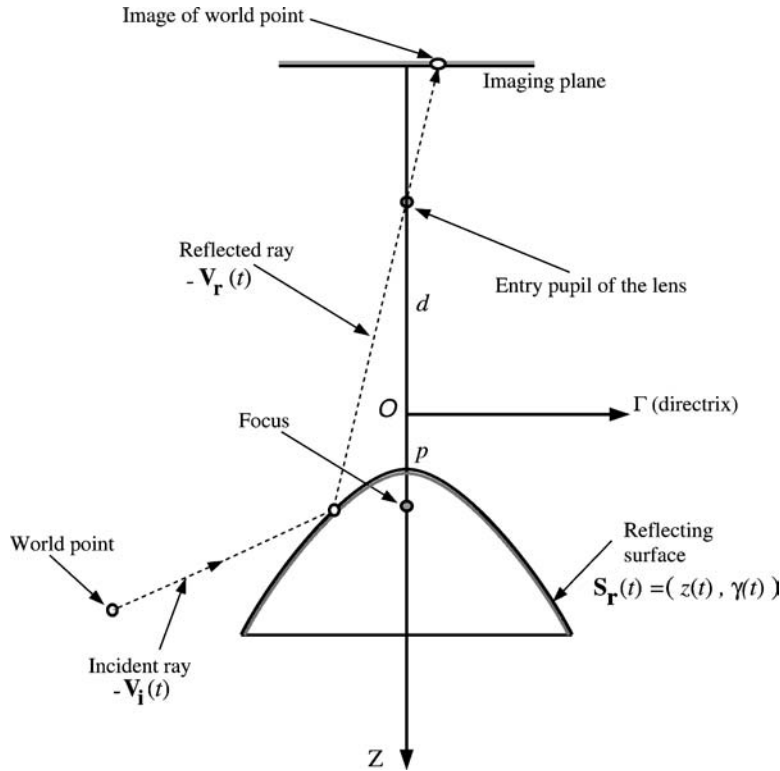


Figure 2. An imaging system consisting of a conic reflector and a perspective lens based camera. The entrance pupil of the lens is located at distance d from the origin, along the axis of symmetry of the conic section. The reflector profile is also defined in this coordinate frame. A light ray from the scene reflects off the reflector surface and is imaged after passing through the entry pupil. A telecentric lens is modeled by taking the limit $d \rightarrow \infty$. Note that this imaging system can have a non-single viewpoint in spite of using a perspective lens.

this approach does not extend to three dimensions as is required in asymmetric systems (see (Swaminathan et al., 2001) for details).

We use the more general definition of caustics as points of singularity in the space of scene rays. Burkhard and Shealy (1973) used this definition and derived a simple Jacobian based constraint to derive the caustic. We use the same approach to derive and analyze caustics of imaging systems.

We first present caustics of rotationally symmetric catadioptric systems, where the entrance pupil of the lens is located along the axis of symmetry of the reflector (see Fig. 2) at a distance d from the origin O . Telecentric lenses are modeled by taking the limit $d \rightarrow \infty$ i.e. modeling an orthographic projection. The reflector profile is also defined in this coordinate frame. Since the system is rotationally symmetric, the analysis reduces to two dimensions (a vertical cross section of the imaging system). However, for rotationally asymmetric systems, we must derive caustics in three dimensions.

2.1.1. The Reflector Surface. Parameterization of the reflector surface is an essential step towards computing the caustic surface analytically. Indeed, whatever the parameterization for the reflector, a solution for the caustic surface exists. We found that standard parameterizations used for conics lead to complicated solutions that are difficult to analyze. In contrast, the following generic parameterization yields a simple solution to the caustic surface. Referring to Fig. 2, we define:

$$\begin{aligned} z(t) &= t \\ \gamma(t) &= \sqrt{(e^2 - 1)t^2 + 2pt - p^2} \end{aligned} \tag{1}$$

where, e is the eccentricity and p the focus of the conic section. This represents elliptic ($e < 1$), parabolic ($e = 1$) and hyperbolic ($e > 1$) reflectors. The vertex of the reflector is given by $\frac{p}{1+e}$. The Γ -axis is the directrix of the conic reflector. A point on the reflector surface is then $\mathbf{S}_r(t) = [z(t), \gamma(t)]$. Although this

parameterization has a singularity for spherical reflectors, it makes it easier to analyze and describe the various geometrical properties of the family of viewpoint loci. In Appendix A, we derive caustics using a more generic parameterization which includes the sphere.

2.1.2. The Rotationally Symmetric Caustic Surface. Figure 2 shows a single reflector based catadioptric system. The entrance pupil of the lens is located d units above the origin as shown. The focal point of the conic reflector lies p units below the origin. A point in the scene is imaged on the detector, after reflecting at some point on the mirror surface. From Fig. 2, the vector along the reflected ray (entering the lens pupil) is given by:

$$\mathbf{V}_r(t) = [t + d, \sqrt{(e^2 - 1)t^2 + 2pt - p^2}]. \quad (2)$$

Since we know the geometry of the reflector, its surface normal $\mathbf{N}_r(\mathbf{t})$ can be derived analytically. Reflecting

$\mathbf{V}_r(t)$ about the surface normal $\mathbf{N}_r(t)$ we derive the pencil of incident rays $\mathbf{V}_i(t)$ as:

$$\mathbf{V}_i(t) = \mathbf{V}_r(t) - 2\mathbf{N}_r(t)(\mathbf{N}_r(t) \cdot \mathbf{V}_r(t)). \quad (3)$$

A point along the incident ray (along $\mathbf{V}_i(t)$) parameterized by its distance r from the point of reflection $\mathbf{S}_r(t)$ is then given by: $\mathbf{S}_r(t) + r \cdot \mathbf{V}_i(t)$. The caustic is tangential to the ray along $\mathbf{V}_i(t)$ and hence for some r_c the caustic point lies at (see Fig. 3):

$$\mathbf{S}_r(t) + r_c \cdot \mathbf{V}_i(t). / \text{vspace} * -3pt \quad (4)$$

A point on the caustic is defined as a singularity in the space of scene rays, parameterized by (r_c, t) (Arnold, 1978). Thus, in the limit, traversing infinitesimally along $\mathbf{V}_i(t)$ (change in r_c) at the caustic, is equivalent to traversing from one ray to the next (change in t). At this point, the determinant of the Jacobian $J(\mathbf{S}_r(t) + r_c \cdot \mathbf{V}_i(t))$ must vanish. Let us now denote the Z and Γ components of $\mathbf{S}_r(t)$ by $\mathbf{S}_r(t)_z$ and $\mathbf{S}_r(t)_\gamma$,

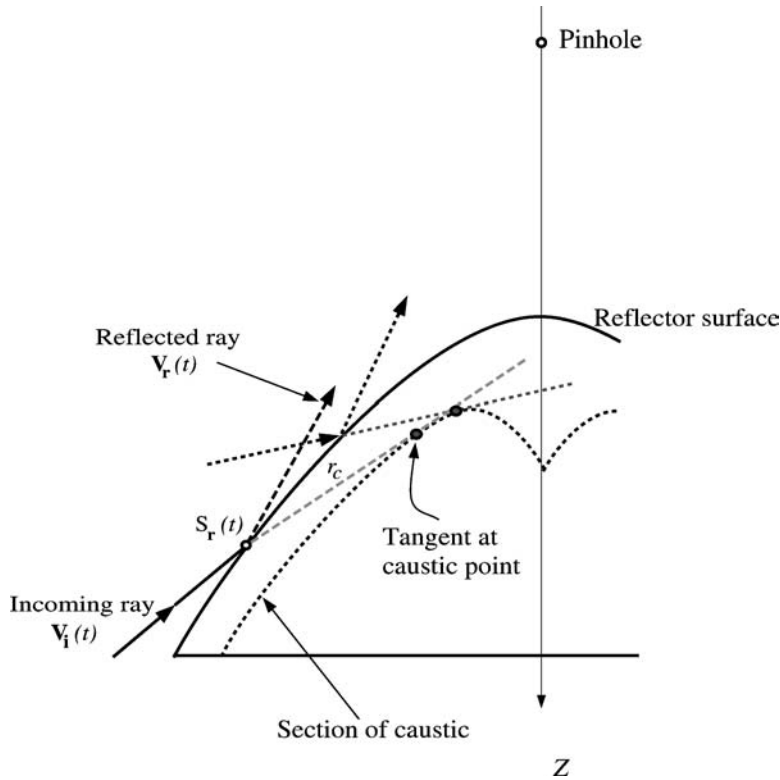


Figure 3. Section of the reflector showing incident rays from the scene reflected into the lens. The incident ray $\mathbf{V}_i(t)$ is tangential to the caustic surface. The distance of the point on the caustic from the point of reflection is denoted by r_c . At the caustic point, if we travel infinitesimally along $\mathbf{V}_i(t)$, we would also move from one ray onto the next. This is because the caustic is also the envelope of the scene rays (incoming rays).

respectively, and those of $\mathbf{V}_i(t)$ by $\mathbf{V}_i(t)_z$ and $\mathbf{V}_i(t)_\gamma$. Enforcing the vanishing constraint on Eq. (5) we get:

$$\det \left(\begin{bmatrix} \dot{\mathbf{S}}_r(t)_z + r_c \cdot \dot{\mathbf{V}}_i(t)_z & \mathbf{V}_i(t)_z \\ \dot{\mathbf{S}}_r(t)_\gamma + r_c \cdot \dot{\mathbf{V}}_i(t)_\gamma & \mathbf{V}_i(t)_\gamma \end{bmatrix} \right) = 0, \quad (5)$$

where, $\dot{\mathbf{S}}_r(t) = \frac{d\mathbf{S}_r(t)}{dt}$ and $\dot{\mathbf{V}}_i(t) = \frac{d\mathbf{V}_i(t)}{dt}$. Solving for r_c we get:

$$r_c(t) = \frac{\dot{\mathbf{S}}_r(t)_\gamma \mathbf{V}_i(t)_z - \dot{\mathbf{S}}_r(t)_z \mathbf{V}_i(t)_\gamma}{\dot{\mathbf{V}}_i(t)_z \mathbf{V}_i(t)_\gamma - \dot{\mathbf{V}}_i(t)_\gamma \mathbf{V}_i(t)_z}. \quad (6)$$

For the class of conic catadioptric cameras, we substitute Eqs. (2, 2) into Eq. (6), to get r_c :

$$r_c(t) = \frac{t(2p + t(e^2 - 1))(t(d(1 - e^2) + p) - p(d + p))}{2p^2(p^2 - d^2) - 6tp^2(d + p) - 3t^2p(d + p)(e^2 - 1) - t^3(e^2 - 1)(d(e^2 - 1)d - p)}. \quad (7)$$

Substituting Eq. (7) in Eq. (4), we get the caustic profile for the family of rotationally symmetric conic catadioptric cameras as a three parameter (e, p, d) family of curves:

$$z_c = \frac{N_z}{D_c}, \quad (8)$$

$$\gamma_c = \frac{N_\gamma}{D_c}, \quad \text{where,}$$

$$\begin{aligned} N_z &= 2p^3(d + p)^2 + 6(d(e^2 - 1) - p)p^2(d + p)t \\ &\quad + 3p(d + p)(d(2 - 3e^2 + e^4) + 2p)t^2 \\ &\quad + (d^2(e^2 - 2)(e^2 - 1)^2 - d(4 - 7e^2 + 3e^4)p \\ &\quad + 2(e^4 + e^2 - 1)p^2)t^3, \end{aligned}$$

$$\begin{aligned} N_\gamma &= 2(d + p)(d - de^2 + p + e^2p) \\ &\quad ((e^2 - 1)t^2 + 2pt - p^2)^{\frac{3}{2}}, \end{aligned}$$

$$\begin{aligned} D_c &= e^2(2(d - p)p^2(d + p) + 6p^2(d + p)t \\ &\quad + 3(e^2 - 1)p(d + p)t^2 + (e^2 - 1) \\ &\quad (d(e^2 - 1) - p)t^3). \end{aligned}$$

The caustic produced due to a telecentric lens and a conic reflector is obtained by taking the limit $d \rightarrow \infty$ in Eq. (8):

$$\begin{aligned} z_c^\infty &= (2p^3 + 6(e^2 - 1)p^2t + 3(2 - 3e^2 + e^4)pt^2 \\ &\quad + (e^2 - 2)(e^2 - 1)^2t^3)/(2e^2p^2), \quad (9) \\ \gamma_c^\infty &= ((1 - e^2)((e^2 - 1)t^2 + 2pt - p^2)^{\frac{3}{2}})/(e^2p^2). \end{aligned}$$

We observe from Eq. (8) that the caustic surface is dependent on the distance d of the entry pupil with respect

to the reflector, the reflector geometry parameterized by eccentricity e , and the focal point p . Since conic reflector based catadioptric systems also produce single viewpoint imaging systems (see Baker and Nayar, 1999), we ask: At what distance d_0 of the entrance pupil would the system produce a point caustic (single viewpoint) at the focus $(d, 0)$ of the reflector? From Eq. (8), we set $z_c = p$, and $\Gamma_c = 0$ and solve for d_0 :

$$d_0 = p \frac{e^2 + 1}{e^2 - 1}. \quad (10)$$

In Eq. (10), setting $e = 1$ (parabolic reflector) gives $d_0 = \infty$, necessitating the use of a telecentric lens as in Nayar (1997). Solutions for elliptical ($e < 1$) and

hyperbolic ($e > 1$) reflectors require the use of perspective lenses located at the focal point of the reflectors. Thus, using the caustic surfaces derived above, we can describe single viewpoint systems as a special case of the general solution.

2.1.3. The Asymmetric Caustic Surface. As noted above, when the imaging system is rotationally symmetric, we can compute its caustic surface as a 2D profile. This simplifies computation and provides a simple solution for the three dimensional caustic surface. However, when the system is not rotationally symmetric, we need to compute the caustic in three dimensions (see Swaminathan et al. (2001) for details). This asymmetry occurs when the entrance pupil is not along the axis of the reflector or the reflector itself is not rotationally symmetric. We now present the derivation of the caustic surface for this generic setting.

Referring to Fig. 4, let $\mathbf{S}_r(t, u)$ be a point on the three dimensional reflector, parameterized by (t, u) . Let \mathbf{O} denote the position of the entrance pupil of the lens. For any such point $\mathbf{S}_r(t, u)$ on the reflector, the direction of the ray entering the pupil can be derived analytically as:

$$\mathbf{V}_r(t, u) = \mathbf{O} - \mathbf{S}_r(t, u). \quad (11)$$

From the known reflector geometry we can derive the vector $\mathbf{V}_i(t, u)$ along the incoming light ray from the reflection equation, similar to Eq. (3).

Again, we denote the distance from the point of reflection at which the caustic lies along \mathbf{V}_i by r_c . The

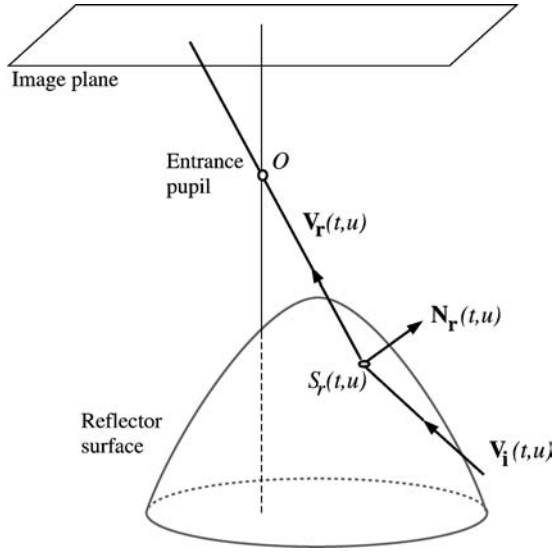


Figure 4. A lens based camera placed off-axis with respect to a rotationally symmetric conic reflector parameterized by (t, u) . The viewpoint locus (caustic surface) of such imaging systems is not rotationally symmetric and hence must be derived in three dimensions. The light ray from the scene $\mathbf{V}_i(t, u)$ reflects off the reflector surface at $\mathbf{S}_r(t, u)$ and is imaged after passing through the entrance pupil O along the reflected ray $\mathbf{V}_r(t, u)$.

caustic surface then is given by:

$$\mathbf{S}_c(t, u) = \mathbf{S}_r(t, u) + r_c \cdot \mathbf{V}_i(t, u) \quad (12)$$

Applying the Jacobian method (Burkhard and Shealy, 1973), we get:

$$\det [J (\mathbf{S}_r(t, u) + r_c \cdot \mathbf{V}_i(t, u))] = 0$$

$$\det \left(\begin{bmatrix} \frac{\partial \mathbf{S}_r(t, u)_X}{\partial t} + r_c \cdot \frac{\partial \mathbf{V}_i(t, u)_X}{\partial t} & \frac{\partial \mathbf{S}_r(t, u)_X}{\partial u} + r_c \cdot \frac{\partial \mathbf{V}_i(t, u)_X}{\partial u} & \mathbf{V}_i(t, u)_X \\ \frac{\partial \mathbf{S}_r(t, u)_Y}{\partial t} + r_c \cdot \frac{\partial \mathbf{V}_i(t, u)_Y}{\partial t} & \frac{\partial \mathbf{S}_r(t, u)_Y}{\partial u} + r_c \cdot \frac{\partial \mathbf{V}_i(t, u)_Y}{\partial u} & \mathbf{V}_i(t, u)_Y \\ \frac{\partial \mathbf{S}_r(t, u)_Z}{\partial t} + r_c \cdot \frac{\partial \mathbf{V}_i(t, u)_Z}{\partial t} & \frac{\partial \mathbf{S}_r(t, u)_Z}{\partial u} + r_c \cdot \frac{\partial \mathbf{V}_i(t, u)_Z}{\partial u} & \mathbf{V}_i(t, u)_Z \end{bmatrix} \right) = 0, \quad (13)$$

where, the X, Y and Z components of the vectors are denoted as $\mathbf{S}_r(t, u)_X$, $\mathbf{S}_r(t, u)_Y$ and $\mathbf{S}_r(t, u)_Z$, respectively. Solving the above equation yields a quadratic equation in r_c , the roots of which give us the analytic solution for r_c . The root of the equation can be substituted in Eq. (12) to derive the analytic form of the caustic in three dimensions. We do not explicitly present this result as the equations are quite unwieldy.

2.2. Examples of Caustic Surfaces

We now present the viewpoint loci for typical conic catadioptric systems. Figures 5(a), (d) and (g) illustrate viewpoint loci (gray curves) for a catadioptric sensor consisting of a perspective lens and an elliptic, a parabolic and an hyperbolic reflector (dark curves), respectively. The dotted curves in Fig. 5(a) denote the part of the elliptic reflector that is self-occluded as well as its corresponding ‘‘virtual-caustic’’. Similarly, Fig. 5(b), (e) and (h) show profiles for catadioptric systems consisting of a telecentric lens and an elliptic, parabolic and hyperbolic reflector, respectively. Note that in Fig. 5(e) the caustic degenerates to a point as expected.

Figure 5(c) is a three-dimensional plot of the caustic surface for a symmetric system consisting of a parabolic reflector and a perspective lens. Figure 5(f) depicts the caustic surface in three dimensions for an asymmetric (pupil not on axis of symmetry) catadioptric system. Figure 5(i) is the viewpoint locus for a catadioptric system including a hyperbolic reflector and a telecentric lens. Unlike the other caustic surfaces that are bounded by their reflectors’ sizes, this caustic surface expands radially.

From the above examples it is clear that the viewpoint locus can be potentially large and at times as large as the reflector itself. To process the image formed by such a system, one must first understand the geometry of the imaging system. The viewpoint locus derived using the framework of caustics completely describes the geometry of the imaging system.

3. Properties of Caustic Surfaces

We now present some characteristic properties of caustics such as surface singularities and field of view along with their relevance to the design of imaging systems. These apply to both convex reflectors and concave reflectors. Most of the observations made are relevant

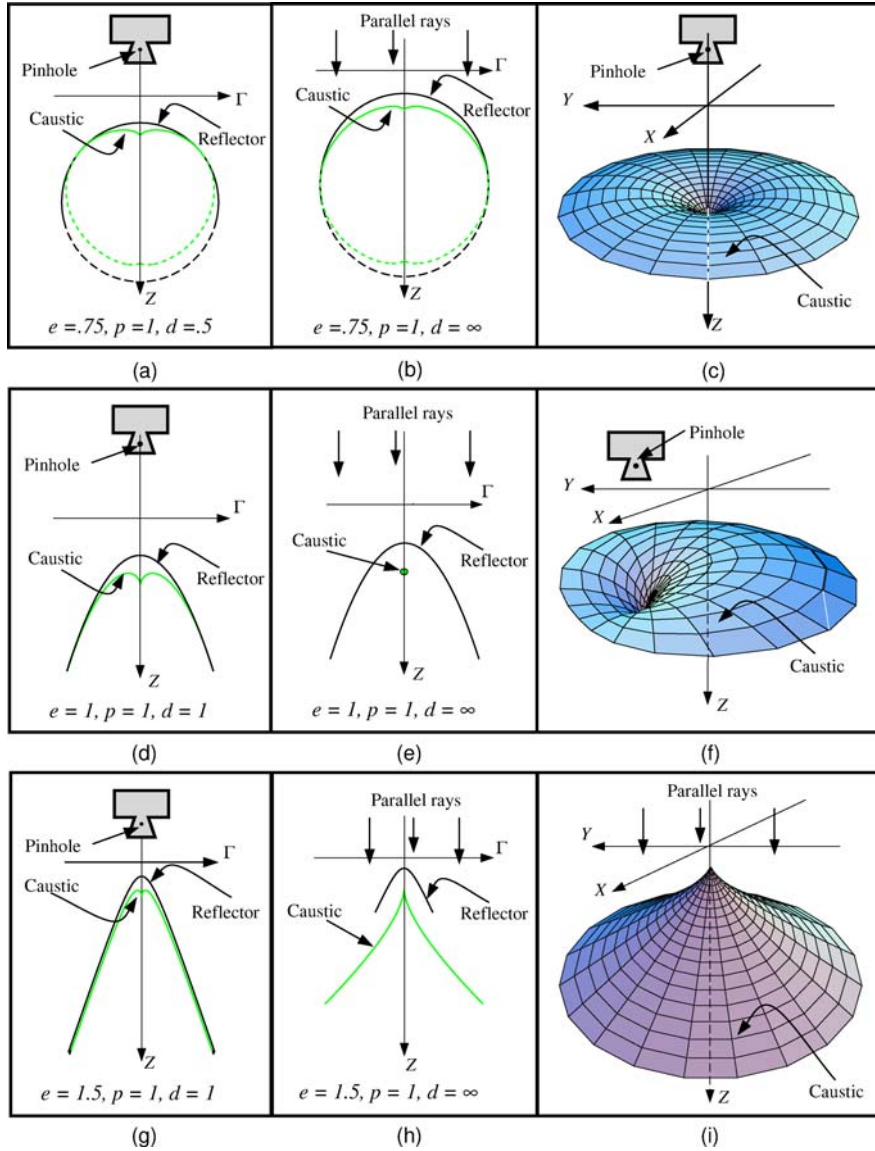


Figure 5. Viewpoint loci for conic catadioptric systems. Column one: Caustics for symmetric systems consisting of a perspective lens and an (a) elliptic, (d) parabolic and (g) hyperbolic reflector. Column two: Viewpoint loci for catadioptric systems consisting of a telecentric lens and an (b) elliptical, (e) parabolic and (h) hyperbolic reflector. Column three: (c) Caustic surface in 3D for a symmetric catadioptric system consisting of a parabolic reflector and perspective lens. (f) Caustic surface for an asymmetric catadioptric camera consisting of an off-axis perspective lens and a parabolic reflector. (i) Caustic surface for a telecentric and hyperbolic reflector system. All caustics were derived using the Jacobian technique described in Section 2.

to both rotationally symmetric as well as asymmetric imaging systems. However, derivations are shown for the rotationally symmetric systems for clarity.

3.1. Singularities on the Caustic Surface

As seen from Fig. 6, caustic surfaces have singularities which we refer to as cusps. These corre-

spond to the points on the reflector where its surface normal coincides with the reflected light ray (along $\mathbf{V}_r(t, u)$) which enters the entrance pupil of the lens (see Fig. 6). This constraint in general is given by:

$$\mathbf{V}_r(t, u) = -\mathbf{N}_r(t, u).$$

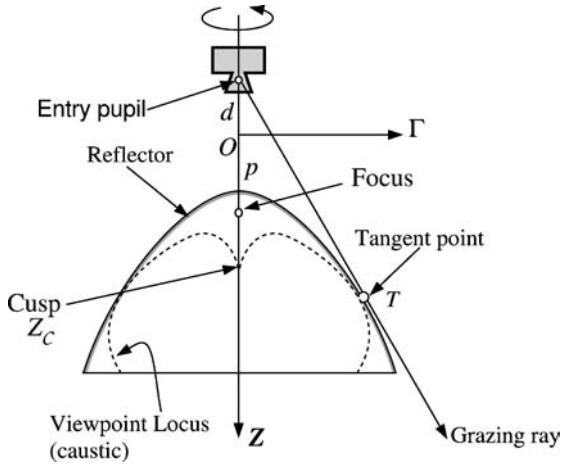


Figure 6. Typical catadioptric camera consisting of a reflector and a perspective lens. The caustic has a singularity denoted by Z_c which we call the cusp. Also shown is the tangent ray to the reflector surface. The point of tangency T is also a point on the caustic surface.

For rotationally symmetric systems with convex or concave reflectors, we get:

$$\mathbf{V}_r(t) = -\mathbf{N}_r(t). \quad (14)$$

In such systems, the cusp lies along the optical axis. Referring to Fig. 6, we only need to compute the Z coordinate of the cusp. From Eqs. (8) and (14) we solve for the Z coordinate of the cusp:

$$Z_c = \frac{p((1+e)(2+e+e^2)d + 2(1+e+e^2)p)}{(1+e)(2(1+e)d + (2+e+e^2)p)}. \quad (15)$$

3.1.1. The Cusp and Rotationally Symmetric Systems.

We now discuss the significance of the cusp to the design of imaging systems whose caustics are rotationally symmetric. We pose the problem of creating a spherical or cylindrical panorama from the image acquired from such a non-single viewpoint sensor. In such cases, a single center of projection is assumed. Since our sensor does not have a single center of projection, parallax effects (due to the multiple viewpoints) are introduced in the panorama called caustic distortions (Swaminathan et al., 2003). The location of the cusp can be used to approximate a single viewpoint to create near perspective views.

We observe that any incoming light ray, which eventually gets imaged by the detector, meets the optical

axis at some point. At the cusp, the light ray passes along the optical axis into the lens. As we move radially outwards, all incoming light rays (tangent to the caustic profile) intersect the optical axis at a point which moves towards the entrance pupil of the lens. Finally, at the very extreme end of the caustic surface, where it touches the reflector, the incoming ray grazes the reflector and meets the optical axis at the entrance pupil. Thus, all the light rays entering the imaging system (tangent to the caustic surface) intersect the optical axis between the entrance pupil and the cusp. The cusp and the entrance pupil therefore bound the possible locations of the virtual center of projection (single viewpoint). More importantly, the density of light rays near the cusp is highest. Thus, more viewpoints lie closer to the cusp than at any other point along the optical axis. This makes the cusp location a good candidate for the single viewpoint approximation.

As the entrance pupil moves closer to the reflector, the cusp moves towards the entrance pupil. However, when the lens moves farther from the reflector, the cusp moves in the opposite direction. In Eq. (15), taking the limit $d \rightarrow \infty$, we find that the position of the cusp converges to:

$$Z_c^\infty = \frac{p(2+e(1+e))}{2(1+e)}. \quad (16)$$

Thus, even if the exact location of the entrance pupil is unknown, one can estimate an upper bound on the cusp's location.

3.2. Caustics and Field of View

Catadioptric systems consisting of convex reflectors have a pencil of rays which graze the reflector surface (see Fig. 7). These rays define the limit of the field of view of the camera. We now show that for reflectors without points of inflection, the point of tangency of the grazing ray on the reflector surface, corresponds to its caustic point.

Theorem 1. *The point on the reflector at which a light ray passing through the entrance pupil pupil of the lens grazes the reflector, is also its caustic point.*

Proof: Let any point on the reflector be given by $\mathbf{S}_r(x, y) = \{x, y, Z(x, y)\}$. Let the position of the entrance pupil of the lens be given by $\mathbf{P} = \{U, V, W\}$.

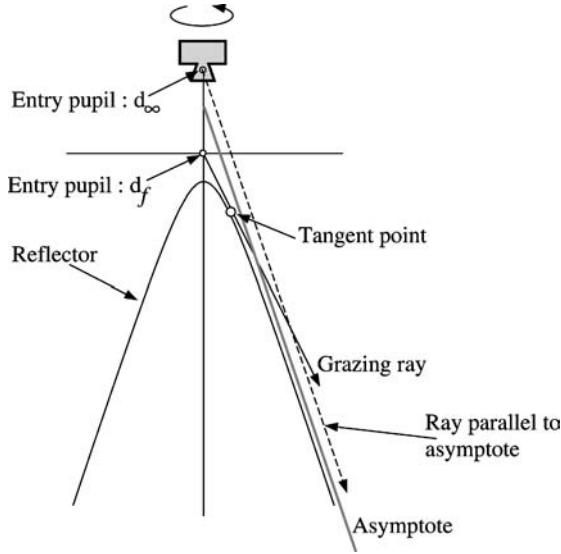


Figure 7. A catadioptric system consisting of an hyperbolic reflector. A entry pupil at d_f possesses a ray which is tangent to the hyperbola at a point along the reflector. However, no light ray entering the pupil d_∞ can be tangential to the reflector.

The light ray entering the pupil is then given by:

$$\mathbf{V}_i(x, y) = \mathbf{S}_r(x, y) - \mathbf{P} \quad (17)$$

For the known reflector, the surface normal is derived as:

$$\mathbf{N}_r(x, y) = \frac{1}{\sqrt{1 + \frac{\partial Z(x, y)^2}{\partial x^2} + \frac{\partial Z(x, y)^2}{\partial y^2}}} \times \left\{ -\frac{\partial Z(x, y)}{\partial x}, -\frac{\partial Z(x, y)}{\partial y}, 1 \right\} \quad (18)$$

Since we know that the reflected ray along $\mathbf{V}_r(x, y)$ grazes the reflector surface, it must lie in the plane tangent to $\mathbf{S}_r(x, y)$. We can thus select an appropriate coordinate frame such that the XY -plane corresponds to the tangent plane, giving $\frac{\partial Z(x, y)}{\partial x} = 0$ and $\frac{\partial Z(x, y)}{\partial y} = 0$. Also, since the pupil \mathbf{P} lies in the XY -plane, we have $W = 0$.

Using the method described in Burkhard and Shealy (1973) we compute the desired Jacobian as:

$$J(\mathbf{S}_r(x, y) + r_c \cdot \mathbf{V}_r(x, y)) = \begin{bmatrix} -U & 1 + r_c & 0 & 0 \\ -V & 0 & 1 + r_c & 0 \\ 0 & -2r_c \left(V \frac{\partial^2 Z(x, y)}{\partial x \partial y} + U \frac{\partial^2 Z(x, y)}{\partial^2 x} \right) & -2r_c \left(V \frac{\partial^2 Z(x, y)}{\partial^2 y} + U \frac{\partial^2 Z(x, y)}{\partial x \partial y} \right) & 0 \end{bmatrix}. \quad (19)$$

Solving for r_c (when the determinant of the Jacobian vanishes) we get:

$$\begin{aligned} r_c &= 0 \\ r_c &= -1 \end{aligned} \quad (20)$$

The solution $r_c = 0$ corresponds to the point of reflection on the reflector. This proves that the caustic point and the point of tangency coincide. \square

We showed that in three dimensions the grazing ray is tangent to the reflector at a point which is also a point on the caustic surface. A similar result has been already shown for caustics of $2D$ curves with respect to a point in a plane (see Bruce et al., 1998).

3.2.1. Location of the Tangent Point. We now derive the exact parametric form for the location of the “tangent point” using the constraint $r_c = 0$ for the class of rotationally symmetric conic catadioptric systems. Setting Eq. (6) to be zero, we solve for the point of tangency parameterized by $t_{r=0}$:

$$t_{r=0} = \frac{p(d+p)}{d+p-de^2}. \quad (21)$$

Within the class of conic reflectors, only hyperbolic mirrors do not always have a grazing ray because the reflector is asymptotic. Referring to Fig. 7, if the entrance pupil of the lens is placed between the vertex of the reflector and the point of intersection between its two asymptotes, a tangent ray (grazing ray) exists which touches the reflector at a finite point. In contrast, if the entrance pupil is located farther away, then there is no tangent ray to the reflector. The caustic of such an imaging system is also asymptotic, and approaches but never touches, the reflector surface.

For conic reflector based catadioptric imaging systems, we observe that the caustic is generally contained within the reflector. Thus, the grazing point on the reflector surface, generally also bounds the caustic size. This bound is important when analyzing distortions due to parallax in “perspective” views computed from images acquired with such non-single viewpoint imaging systems.

4. Resolution

So far we analyzed the geometry of the viewpoint surface, its singularities and its field of view. We now analyze the effect of such viewpoint surfaces on the resolution characteristics of the sensor. We derive an analytic expression for resolution and show how small changes in the design impact resolution dramatically. Baker and Nayar (1999) showed that conic reflector based single viewpoint catadioptric cameras possess radially increasing resolution. Such imaging systems are a special case of conic catadioptric cameras. We now extend their analysis to include non-single viewpoint imaging systems as well.

4.1. Single Reflector with Perspective Lens

Consider an infinitesimal area δA in the imaging plane. The angle subtended by this region about the entrance pupil is ψ . Let this area image an infinitesimal solid angle $\delta\omega$ of the scene (see Fig. 8). The resolution of the imaging system is then defined as $\frac{\delta A}{\delta\omega}$. Thus, smaller

the solid angle visible at the infinitesimal region δA , greater is the resolution of the imaging system.

The distance of the image point corresponding to the elemental area δA from the entrance pupil is: $f/\cos(\psi)$. Then, the solid angle subtended by the foreshortened area $\delta A \cos(\psi)$ at the entrance pupil of the lens is:

$$\delta\vartheta = \frac{\delta A \cos^3(\psi)}{f^2}, \quad (22)$$

where f is the focal length of the lens. The area projected onto the reflector by δA can then be derived using the solid angle $\delta\vartheta$ as:

$$\delta S = \frac{\delta A \cos(\psi)(d + z(t))^2}{(f^2 \cos(\phi))}, \quad (23)$$

where, ϕ is the angle between the principal ray corresponding to δA and the surface normal at δS . The foreshortened area visible to the viewpoint (of the principal

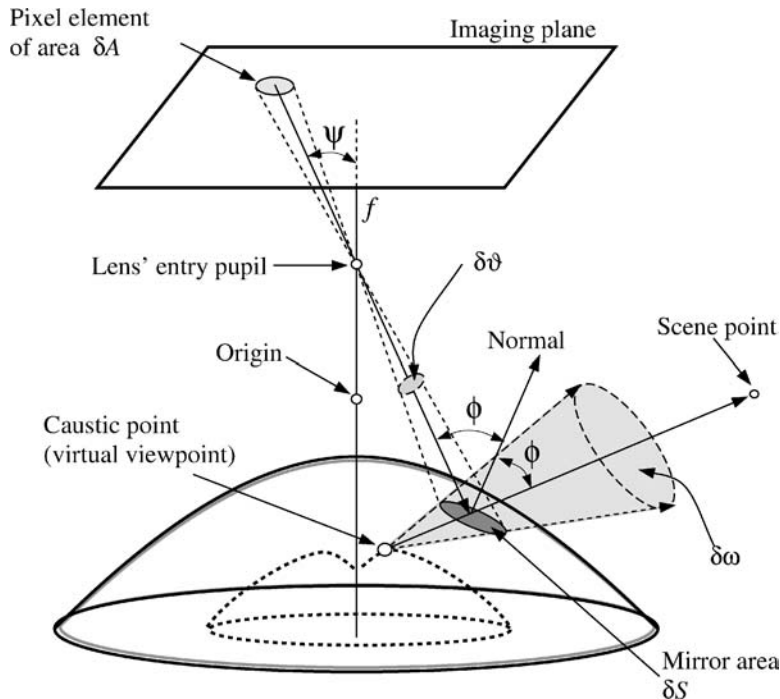


Figure 8. A pixel element of area δA in the image plane projects through the entry pupil of the lens onto the reflector as a region of area δS . The pupil is located at $(0, 0, d)$, with respect to the origin. The principal ray from δA reflects off the reflector at $s_R(x(t, \theta), y(t, \theta), z(t, \theta))$. The corresponding viewpoint on the caustic surface as shown above. The solid angle subtended at this viewpoint is then $\delta\omega = \delta S/r_c^2$, where r_c is the distance of the viewpoint from the reflector (see Eq. (6)). Resolution is then defined as a ratio of $\delta\omega$ to δA .

ray) on the caustic surface is therefore:

$$\frac{\delta A \cos(\psi)(d+z(t))^2}{f^2}. \quad (24)$$

The solid angle subtended at this caustic point is then given by:

$$\delta\omega = \frac{\delta A \cos(\psi)(d+z(t))^2}{f^2 \cdot r_c(t)^2}, \quad (25)$$

where, $r_c(t)$ is the distance of the viewpoint from the reflector surface (see Eq. (7)). The resolution for any rotationally symmetric catadioptric camera is then given by:

$$\frac{\delta A}{\delta\omega} = \frac{f^2 \cdot r_c(t)^2}{\cos(\psi)(d+z(t))^2}. \quad (26)$$

Substituting Eq. (7) in Eq. (26) we obtain the expression for resolution of a rotationally symmetric conic catadioptric system.

We now present the resolution characteristics for some configurations of conic catadioptric cameras. These consist of a conic reflector (whose profile is a conic section) and a perspective lens system, whose entrance pupil is located at a finite distance from the reflector. The resolution results presented are only for rotationally symmetric systems.

Figure 9 illustrates the resolution across a radial slice of the imaging plane. The curves have been normalized with respect to magnification such that the total

field of view in all three cases are the same. This facilitates a fair comparison of resolution between the three catadioptric systems. As seen, resolution drops drastically beyond some distance from the image center. This characteristic gradually changes as entry pupil approaches the focal point of the reflector (the system becomes single viewpoint). For this configuration, the resolution increases radially, consistent with Baker and Nayar (1999).

We now give an intuitive explanation as to why resolution tends to drop towards the edge of the caustic. Typically, the caustic approaches the reflector surface radially outwards. Eventually the caustic touches the reflector at the ‘‘tangent point’’. Thus, $r_c \rightarrow 0$ and hence the solid angle subtended increases (see Eq. (25)), reducing resolution. In contrast with single viewpoint systems, r_c increases as we move radially outwards, thus increasing resolution.

4.2. Single Reflector with Telecentric Lens

We now discuss a catadioptric imaging system consisting of a telecentric lens and a single conic reflector. From Fig. 10, projection of the area δA in the imaging plane onto the reflector is $\delta A / \cos(\phi)$. The foreshortened patch which is visible from the viewpoint on the caustic surface is δA . The solid angle subtended at this viewpoint is given by:

$$\delta\omega^\infty = \frac{\delta A}{r_c^\infty{}^2}, \quad (27)$$

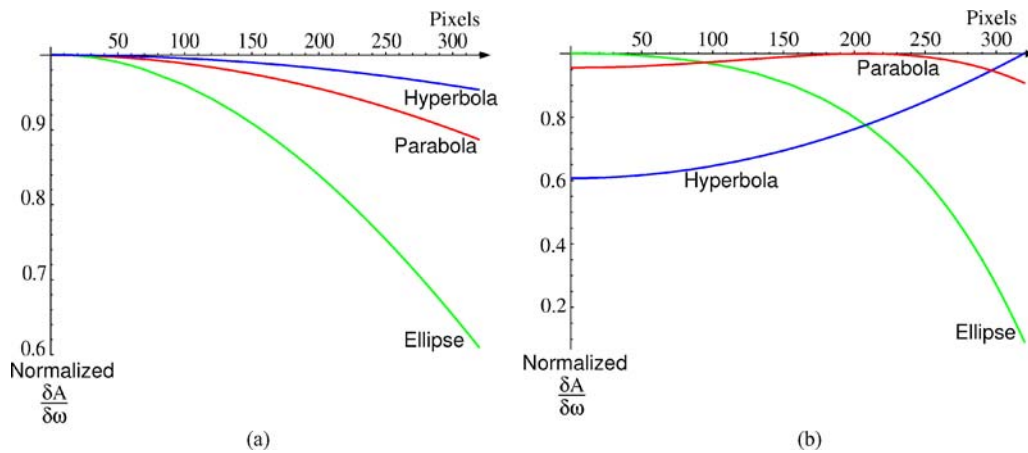


Figure 9. Plots of resolution for catadioptric sensors having a perspective lens based camera and an elliptic, a parabolic and an hyperbolic reflector. The plots illustrate the resolution across a radial slice of the image plane when the pupil is located at (a) the origin ($d = 0$) and (b) at $d = 6$.

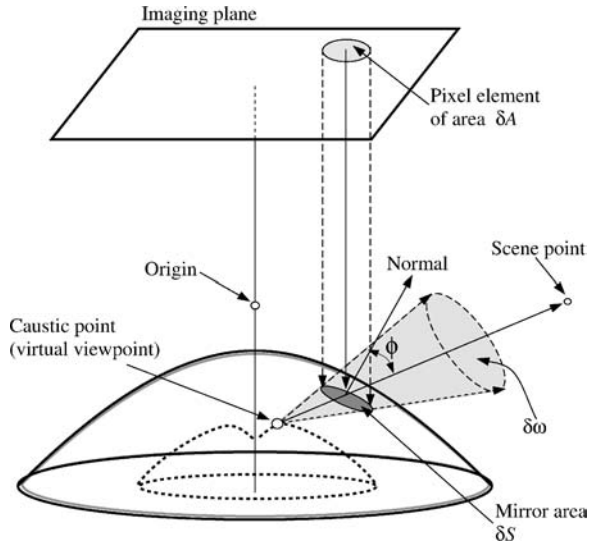


Figure 10. A pixel element of area δA in the image plane projects through the telecentric lens (orthographic projection) onto the reflector as a region of area δS . The principal ray from δA (corresponding to the center of the area δA) reflects off the mirror at $s_R(x(t, \theta), y(t, \theta), z(t, \theta))$. The corresponding viewpoint on the caustic surface is as shown above. The solid angle subtended at this viewpoint is then $\delta\omega = \delta S/r_c^2$, where r_c is the distance of the viewpoint from the reflector (see Eq. (6)). Resolution is then defined as a ratio of $\delta\omega$ to δA .

where, r_c is the distance of the viewpoint from the point of reflection on the reflector. If \mathcal{M} is the magnification factor (see Baker and Nayar, 1999), resolution of such

a sensor is given by:

$$\frac{\delta A}{\delta\omega^\infty} = \mathcal{M} \cdot r_c^{\infty 2}. \quad (28)$$

For conic reflectors, the distance of the viewpoint from the point of reflection is given by:

$$r_c^\infty = -\frac{(t(p + (e^2 - 1)t)(2p + (e^2 - 1)t))}{(2p^2)}. \quad (29)$$

Then, resolution for a conic catadioptric imaging system with a telecentric lens is:

$$\frac{\delta A}{\delta\omega^\infty} = \mathcal{M} \cdot \frac{(t(p + (-1 + e^2)t)(2p + (-1 + e^2)t))^2}{4p^4}. \quad (30)$$

We now apply results derived in Eq. (30) to conic catadioptric cameras fitted with a telecentric lens and study their resolution characteristics (see Fig. 11).

For parabolic reflectors, the caustic reduces to a single point (see Baker and Nayar, 1998, 1999). Thus, the resolution increases radially as expected. The caustic surface for an elliptical reflector with telecentric lens is similar in form to that with a perspective lens. Hence, the resolution characteristics are also similar, exhibiting an initial rise and then a drop towards the periphery. Finally, the hyperbolic reflector yields a caustic which expands (see Fig. 5(i)) in a direction opposite to that of

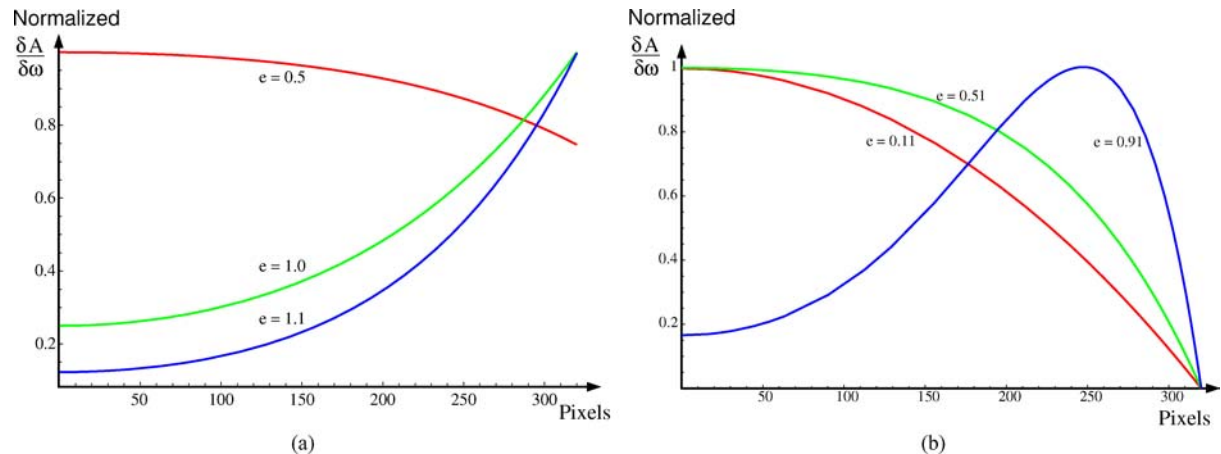


Figure 11. (a) Resolution across a radial slice of the image plane by a catadioptric sensor consisting of a telecentric lens and a parabolic, elliptic and hyperbolic reflector respectively. The resolution plots have been normalized to illustrate the manner in which resolution changes across the image plane. (b) For an elliptic reflector based catadioptric cameras, the resolution always drops to zero at the periphery of the field of view. This drop to zero corresponds to the point on the reflector at which the caustic surface touches it (see Eq. (21)). However, there is no such all in resolution for the case with parabolic or hyperbolic reflectors.

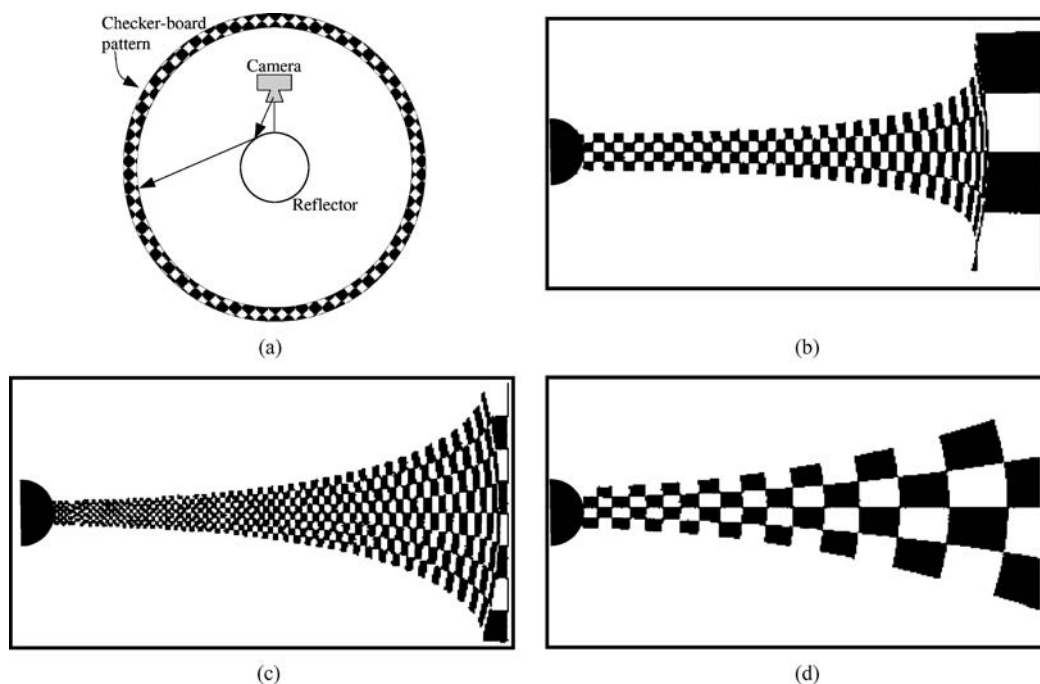


Figure 12. (a) Setup to synthesize images of a catadioptric camera viewing a cylinder that has a checkerboard pattern on its inside. A radial section of the acquired image using a perspective lens and (b) an elliptic reflector and (c) a parabolic reflector. In both cases, the checkerboard pattern initially increases in size then flattens to a curve at the periphery due to the drop in resolution. Note that the checkerboard pattern, at the right edge of the image, is the actual cylinder seen past the reflector. (d) Radially increasing checkerboard pattern due to the single viewpoint maintained by a parabolic reflector and telecentric lens-based imaging system.

the point of reflection. This results in radially increasing resolution.

Figure 12(b)–(d) show the changing resolution by imaging a checkerboard pattern across the field of view. To avoid potential errors in calibration of such non-single viewpoint catadioptric sensors, we used a rendering system to synthesize images. As shown in Fig. 12(a), the catadioptric sensor was placed at the center of a narrow cylinder whose insides have a checkerboard pattern. The small checkerboard pattern is reflected by the mirror, into the lens based camera. Sections of the rendered images are shown in Fig. 12(b)–(d) and correspond to sensors utilizing an elliptic reflector and perspective lens, a parabolic reflector and perspective lens, and a parabolic reflector with telecentric lens, respectively.

As predicted, resolution for the elliptic reflector based sensor (see Fig. 12(b)), rises and then drops at the periphery. Similarly, in Fig. 12(c), the resolution for the parabolic reflector with perspective lens drops at the periphery (tangent point on reflector). This is observed by the increase of the area of the rectangles in the image, finally getting compressed to a thin strip

at the periphery. However, in Fig. 12(d), the parabolic reflector with telecentric lens based sensor has an increasing resolution similar to our prediction and that by Baker and Nayar (1999).

4.3. Designing Resolution Specific Sensors

The analytic expressions for resolution of catadioptric cameras are not restricted to conic reflectors alone. In general, the same framework can be extended to any mirror shape. Moreover, the formulae derived above not only aids in analyzing the resolution of the sensor, but can also be used to drive the system's design (Hicks and Perline, 2002; Gaspar et al., 2002; Gachter et al., 2001).

Consider the class of conic catadioptric systems for which resolution is parameterized by the geometry of the reflector. Given an a priori resolution curve, we can “fit” the right parameters in the model (e, p, d, f) , that most closely approximate the required curve. In general setting, we could estimate any parametric reflector shape for a prescribed resolution characteristic.

It should however be noted that by fixing the resolution, the imaging system need not maintain a single viewpoint.

5. Self-Calibration of Non-Single Viewpoint Cameras

So far we discussed the geometry and resolution characteristics of conic catadioptric imaging systems. We derived a parametric expression for their viewpoint loci in terms of the geometry and location of the various imaging components. If the exact geometry and configuration of the imaging components such as lenses and mirrors is known, the caustic or viewpoint locus can be derived analytically. However, when these parameters are unknown, self-calibration is required. Although every pixel has a unique viewpoint and viewing direction, the caustic formulation reduces the complexity of calibration to that of estimating only a handful of parameters.

In the past, techniques for calibrating single viewpoint catadioptric systems have been suggested using a single image (Geyer and Daniilidis, 1999) or cam-

era motion (Kang, 2000). Recently, Grossberg and Nayar (2001) suggest using caustics to represent generic imaging systems, and also presented a calibration technique which uses known motion as well as known scene points using an active display of known light patterns. In contrast, our technique calibrates non-single viewpoint systems having a parametric form for the caustic, using only known camera motion and point correspondences between views of *unknown* scene points by estimating the model parameters.

5.1. Objective Function Formulation

We pose the caustic estimation problem as one of error minimization. As shown in Fig. 13, let p_1 and p_2 be the images of a static scene point P , in the two views. From the hypothesized parameter values (during search), we map p_1 and p_2 to their corresponding viewpoints (S_1 and S_2) as well as their viewing directions (V_1 and V_2). Camera motion is not the only factor that contributes to a new viewpoint. Since the image is formed by reflection from a curved surface, the second view is reflected from a different point on

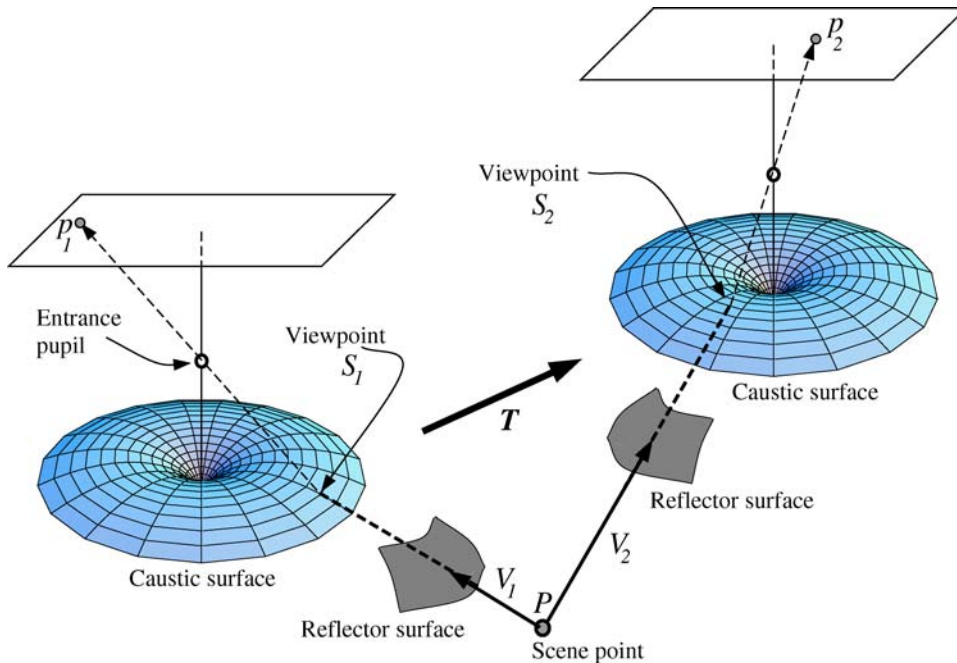


Figure 13. The catadioptric imaging system is represented here by only its caustic surface (viewpoint locus). The two caustic surfaces denote the same camera after being given a known translation T . An unknown scene point P visible from both views gets imaged at two point p_1 and p_2 respectively. From the caustic model and the hypothesized parameters during search, we map these image point to their respective viewpoint S_1 and S_2 and their viewing directions V_1 and V_2 . When the right model parameters are estimated, the two position vectors (light rays at viewpoints) must meet at the scene point.

the reflector. This maps to a different position on the caustic as illustrated in Fig. 13. Since the two light rays come from the same scene point, they must intersect at the scene point. This happens when the hypothesized caustic parameters match that of the system.

In general, we can define the objective function as the distance between these two rays. However, we found it more stable to define the error function in the image space. To do so, we first derive in closed form, a point \tilde{P} along \mathbf{V}_1 which is closest to ray \mathbf{V}_2 (this is the best estimate of the scene point P). This hypothesized scene point \tilde{P} is then mapped onto the image plane in the second view, using the caustic model. We then define the error as the disparity between the image of \tilde{P} in the second view \tilde{p}_2 and known image in the p_2 :

$$\epsilon = \|\tilde{p}_2 - p_2\|_2 \quad (31)$$

The objective function is defined over all the pairs of point correspondences between the two views. Thus, if p_i^j refers to the i th image point in view j , then the objective function for N scene points is given by:

$$\xi = \sum_{\forall i \in N} |\tilde{p}_i^2 - p_i^2|_2 \quad (32)$$

5.2. Calibrating a Real Sensor

We now present calibration results on a real non-single viewpoint catadioptric sensor. The sensor consists of

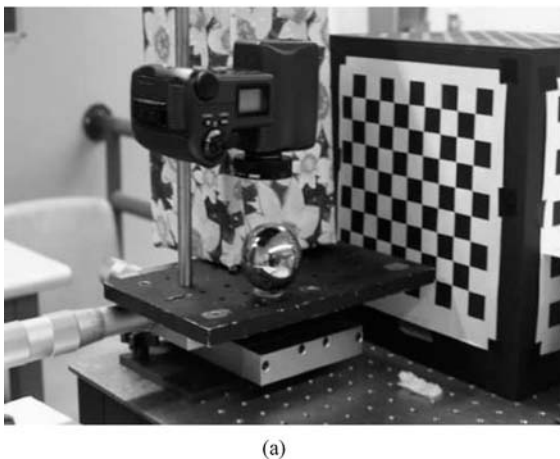
a perspective lens based high resolution digital camera and a spherical reflector (ball bearing). The reflector was two inches in diameter and was placed approximately 150 mm below the digital camera (see Fig. 14(a)). The catadioptric camera was placed rigidly on a translation stage to facilitate accurate camera motions. Between acquiring the two views, the sensor was translated precisely by 20 mm sideways (along the Y axis). Figure 14(b) shows a typical image acquired by this catadioptric sensor.

Since the parameterization in Section 2 is singular for a sphere, we parameterize used an implicit definition of the mirror profile as:

$$A \cdot z^2 + \gamma^2 + B \cdot z = C. \quad (33)$$

which includes the entire class of conic reflectors. As before, the entrance pupil is at a distance d from the origin along the Z axis. The caustic surface is then described by a four-parameter (A, B, C, d) family of curves (see Appendix A).

It should be noted that the robustness of the algorithm depends on the number of free parameters of the caustic model to be estimated. Furthermore, it is imperative that the chosen point correspondences come from scene points that are close to the imaging system. Just like in stereo, parallax effects diminish with greater distance from the imaging system, thereby minimizing image disparity produced by the the viewpoint locus. In our experiment, we used 41



(a)



(b)

Figure 14. (a) A catadioptric camera consisting of a perspective lens based digital camera and a spherical reflector (ball-bearing). The reflector's radius is 25.4 mm, and lens' entry pupil is approximately 150 mm above the center of the sphere. The catadioptric camera was placed on a translation stage and translated by 20 mm along the Y axis. (b) Sample image acquired during the calibration process. Each image is 2048×1536 in size. We used 41 feature points across a 180 degree field of view to calibrate the imaging system.

	\sqrt{C} (mm)	d (mm)	f (pixels)
Ground Truth	25.4	150	5381
Estimated Values	24.7	176.9	5379

Figure 15. Estimated and ground truth parameters for the catadioptric camera shown in Fig. 14. The estimation was done using constrained minimization routines in Matlab.

scene points (image correspondences) to guide the non-linear search. Since we know the reflector to be spherical we only need to estimate the focal length f of the perspective lens, the distance d of the lens's entrance pupil from the reflector, and the radius \sqrt{C} of the reflector.

Figure 15 provides a comparison between the estimated model parameters and the ground truth. The ground truth is based on careful manual measurement of the required model parameters including the radius of the sphere, its distance from the entrance pupil and the focal length of the perspective cameras used in the setup. These parameters determine the ground truth caustic profile plotted in Fig. 16.

The radius of the reflector, estimated using our two view based calibration method, is accurate to within a few millimeters. The estimated focal length is also close to the ground truth. However, the estimate of d is less accurate. This is either due to incorrect convergence of the non-linear search or due to inaccuracy in the measurement of the ground truth. Once the model parameters are estimated we can plot the viewpoint locus for the estimated caustic profile (dotted curve) against ground truth (solid curve) (see Fig. 16).

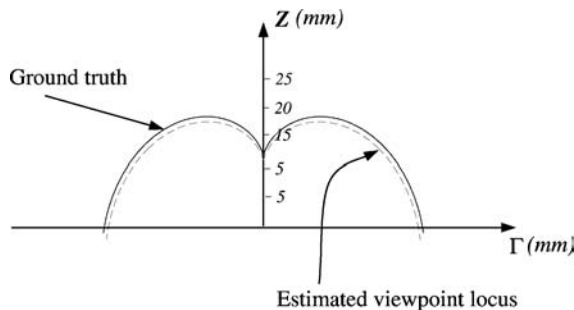


Figure 16. Ground truth (solid curve) and estimated caustic (dotted curve) for the imaging system shown in Fig. 14. As seen, the error in the estimated viewpoint locus of the camera is marginal and follows the ground truth caustic closely.

6. Summary

For a while it has been considered necessary for imaging sensors to maintain a single viewpoint. In reality this limits the flexibility one has in designing optical systems. For instance, we know only conic reflectors provide single viewpoint catadioptric systems. Thus, one must use an elliptical, parabolic or hyperbolic reflector with specific lenses (perspective of telecentric). Also, such imaging systems require precise alignment of the various imaging components, without which the system deviates strongly from a single viewpoint.

If we deviate from the single viewpoint constraint, then we have much more flexibility in designing imaging systems. For instance, we are no longer limited to using only conic reflectors. More exotic reflectors could be used to develop new sensors. This paper presents a step towards understanding such non-single viewpoint imaging systems. We focused on conic reflectors not only because most catadioptric systems utilize such reflectors but also because locally any surface can be approximated by quadrics.

We derived a concise analytic expression for the loci of viewpoints (caustics) of catadioptric imaging systems utilizing conic reflectors. In such imaging systems, every pixel has a unique viewpoint. Using the framework of caustics, the viewpoint surface can be parameterized with a small number of parameters. These parameters depend on the surface geometry of the reflector and the relative location of the entrance pupil of the lens with respect to the reflector. Under this general framework, the single-viewpoint catadioptric camera was also shown to be a special case of the general solution. Any imaging system, whose components (lenses and reflectors) are completely known, can be replaced by the caustic surface for the purposes of analysis.

Apart from deriving an analytic expression for the caustic surface, we also studied other geometric properties of the sensor. For instance, it was shown that the cusp formed along the optical axis for rotationally symmetric systems was closely related to approximating the entire caustic surface by a single point. We also proved that the caustic associated with the tangential light ray to the reflector lies at the point of tangency. This ‘‘tangent point’’ was solved for in closed form giving a good bound on the size of the caustic.

An important reason to relax the single viewpoint is to design imaging systems with specific resolution characteristics. We provide a simple analytic study of

resolution for the class of conic catadioptric imaging systems. We showed how resolution degrades radially beyond some distance from the image center, if the effective viewpoint locus is not a single point. However, careful design of the imaging system in terms of lens and reflector choice and their relative positioning, can be used to exploit the initial rise or plateau effect on resolution. Further the analytic form for resolution can be used to optimize the design parameters of the imaging system for a priori resolution requirements.

Finally, we presented a simple calibration technique to estimate the viewpoint surface and camera parameters for a conic catadioptric system using known camera motion. In general, the problem of calibrating non-single viewpoint cameras is that of estimating a map between each pixel in the image and its unique viewpoint and viewing direction. Using the framework of caustics this potentially hard problem was reduced to that of estimating a small number of model parameters. Although we assumed knowledge of the reflector shape (conic cross-section), the precise geometry of the reflector and camera as a whole was unknown and was estimated from two images of an arbitrary scene.

Appendix A

We now derive the caustic surface for a parameterized conic reflector given by:

$$Az^2 + \gamma^2 + Bz = C. \quad (34)$$

This parameterization not only includes parabolic ($c = 0, A = 0$), elliptic ($B = 0$) and hyperbolic ($A < 0, C < 0$) reflectors, but also spherical ($A = 1, C + \frac{B^2}{4} > 0$). As opposed to Eq. (2) which did not model spherical reflectors, Eq. (34) includes the sphere as well.

In parametric form, Eq. (34) can be rewritten as:

$$\begin{aligned} z(t) &= t \\ \gamma(t) &= \sqrt{C - Bt - At^2} \end{aligned} \quad (35)$$

Using the Jacobian method (Burkhard and Shealy, 1973) we derive the caustic profile as a parametric curve:

$$\begin{aligned} N_z(t) &= B^3C^2 + 6B^2Cd - 4BC^2d + 8Bd^2 - 8Cd^2 \\ &\quad - 3(B - 2A^2C)(B^2C + 4Bd - 4Cd)t \\ &\quad + 6(B^3 - 2(1 + A^2)B^2C + 2A^2(1 + A^2)BC^2 \\ &\quad + 4A^2(A^2 - 1)Cd)t^2 + 4((2A^2 - 1)B^2, \\ &\quad - A^2(1 + 3A^2)BC + 2A^4(1 + A^2)C^2 \end{aligned}$$

$$\begin{aligned} &+ 4A^2(A^2 - 1)d)t^3, \\ N_\gamma(t) &= 4(B^2 - 4BC - 4d + 4A^2(C^2 + d)) \\ &\quad (d - t(B + A^2t))^{3/2} \\ D(t) &= -B^3C + 4B^2C^2 + 2B^2d - 4BCd \\ &\quad + 16A^2C^2d - 8d^2 + 16A^2d^2 \\ &\quad - 3(B^3 + 2(A^2 - 2)B^2C + 4(2A^2 - 1)Bd \\ &\quad - 8A^2Cd)t - 12A^2(A^2 - 1)(BC + 2d)t^2 \\ &\quad + 4A^2(A^2 - 1)(B - 2A^2C)t^3, \\ Sc'(t) &= \left\{ \frac{N_z(t)}{D(t)}, \frac{N_\gamma(t)}{D(t)} \right\}. \end{aligned} \quad (36)$$

Equation (36) describes the caustic profile for the complete class of conic (including spherical) catadioptric cameras. In calibrating such non-single viewpoint imaging systems, when the reflector shape is not known, we should use the above derived model.

Acknowledgments

This work was supported in parts by a National Science Foundation ITR Award, IIS-00-85864, and the DARPA Human Identification (HID) Program, Contract No N00014-00-1-0929. The authors would like to acknowledge Prof. P.J. Giblin of University of Liverpool for his help through many email discussions. We would also like to thank the reviewers for their many indispensable suggestions.

Notes

1. A telecentric lens yields an orthographic projection of the scene onto the image detector.
2. Depending on the local curvature of the reflector surface, bundles of rays diverge to different degrees causing blurring in the image.

References

- Arnold, V. 1978. *Mathematical Methods of Classical Mechanics*. Springer-Verlag.
- Baker, S. and Nayar, S.K. 1998. A theory of catadioptric image formation. In *Proc. ICCV*, pp. 35–42.
- Baker, S. and Nayar, S.K. 1999. A theory of single-viewpoint catadioptric image formation. *IJCV*, 35(2):1–22.
- Bogner, S. 1995. Introduction to panoramic imaging. In *IEEE SMC Conference*, vol. 54, pp. 3100–3106.
- Bolles, R.C., Konolige, K.G., and Fischler, M.A. 1997. Extra set of eyes. In *DARPA-IUW*, pp. 41–44.

- Born, M. and Wolf, E. 1965. *Principles of Optics*. Pergamon Press.
- Bruce, J.W., Giblin, P.J., and Gibson, C.G. 1981. On caustics of plane curves. *American Mathematical Monthly*, 88:651–667.
- Burkhard, D.G. and Shealy, D.L. 1973. Flux density for ray propagation in geometrical optics. *Journal of the Optical Society of America*, 63(3):299–304.
- Chahl, J. and Srinivasan, M. 1997. Reflective surfaces for panoramic imaging. *Applied Optics*, 36(31):8275–8285.
- Charles, J., Reeves, R., and Schur, C. 1987. How to build and use an all-sky camera. *Astronomy Magazine*.
- Derrien, S. and Konolige, K. 2000. Approximating a single viewpoint in panoramic imaging devices. In *International Conference on Robotics and Automation*, pp. 3932–3939.
- Gachter, S., Pajdla, T., and Micusik, B. 2001. Mirror design for an omnidirectional camera with space variant imager. In *Overviews of the Workshops on Omnidirectional Vision*, pp. 99–105.
- Gaspar, J., Decco, C., Okamoto, J. Jr., and Santos-Victor, J. 2002. Constant resolution omnidirectional cameras. In *Proc. OMNIVIS*, p. 27.
- Geyer, C. and Daniilidis, K. 1999. Catadioptric camera calibration. In *Proc. ICCV*, pp. 398–404.
- Gluckman, J. and Nayar, S.K. 1999. Planar catadioptric stereo: Geometry and calibration. In *Proc. CVPR*, pp. I:22–28.
- Grossberg, M. and Nayar, S. 2001. A general imaging model and a method for finding its parameters. In *Proc. ICCV*, pp. 108–115.
- Hamilton, W.R. 1828. Theory of systems of rays. *Transactions of the Royal Irish Academy*, 15:69–174.
- Hicks, A. 2002. Differential methods in catadioptric sensor design with applications to panoramic imaging. Technical report, Drexel University, Computer Science.
- Hicks, R. and Bajcsy, R. 2000. Catadioptric sensors that approximate wide-angle perspective projections. In *Proc. CVPR*, pp. I:545–551.
- Hicks, R. and Perline, R. 2002. Equi-areal catadioptric sensors. In *Proc. OMNIVIS*, p. 13.
- Hong, J.W., Tan, X., Pinette, B., Weiss, R., and Riseman, E.M. 1990. Image-based navigation using 360 views. In *DARPA-IUW*, pp. 782–791.
- Jensen, H.W. 1996. In <http://graphics.stanford.edu/henrik/images/caustics.html>
- Kang, S.B. 2000. Catadioptric self-calibration. In *Proc. CVPR*, pp. I:201–207.
- Murphy, J. 1997. Application of panoramic imaging to a teleoperated lunar rover. In *IEEE SMC Conference*, vol. 36, pp. 3117–3121.
- Nalwa, V. 1996. A true omnidirectional viewer. Technical report, Bell Laboratories, Holmdel, NJ 07733, U.S.A.
- Nayar, S.K. 1997. Catadioptric omnidirectional cameras. In *Proc. CVPR*, pp. 482–488.
- Nayar, S.K. and Karmarkar, A.D. 2000. 360 × 360 Mosaics. In *Proc. CVPR*, pp. I:388–395.
- Pajdla, T. 2001. Epipolar geometry of some non-classical cameras. In *Computer Vision Winter Workshop*, pp. 223–233.
- Pajdla, T. 2002. Stereo with oblique cameras. *Trans. IJCV*, 47(1–3):161–170.
- Peleg, S., Pritch, Y., and Ben-Ezraet, M. 2000. Cameras for stereo panoramic imaging. In *Proc. CVPR*, pp. I:208–214.
- Peri, V.N. and Nayar, S.K. 1997. Generation of perspective and panoramic video from omnidirectional video. *DARPA-IUW*, pp. I:243–245.
- Rees, D. 1970. Panoramic television viewing system. United States Patent No.3,505,465.
- Seitz, S. 2001. The space of all stereo images. In *Proc. ICCV*, pp. I:26–33.
- Srinivasan, M. 2003. New class of mirrors for wide-angle imaging. In *Proc. OMNIVIS*.
- Swaminathan, R., Grossberg, M., and Nayar, S. 2003. A perspective on distortions. In *Proc. CVPR*, pp. II: 594–601.
- Swaminathan, R., Grossberg, M.D., and Nayar, S.K. 2001. Caustics of catadioptric cameras. In *Proc. ICCV*, pp. II:2–9.
- Swaminathan, R., Grossberg, M.D., and Nayar, S.K. 2001. Non-single viewpoint catadioptric cameras: Geometry and analysis. Technical Report CUCS-004-01, Dept. of Computer Science, Columbia University.
- Weinshall, D., Lee, M., Brodsky, T., Trajkovic, M., and Feldman, D. 2002. New view generation with a bi-centric camera. In *Proc. ECCV (1)*, pp. 614–628.
- Yagi, Y., Kawato, S., and Tsuji, S. 1994. Real-time omnidirectional image sensor (copis) for vision-guided navigation. *Robotics and Automation*, 10(1):11–22.
- Yagi, Y. and Yachida, M. 1991. Real-time generation of environmental map and obstacle avoidance using omnidirectional image sensor with conic mirror. In *Proc. CVPR*, pp. 160–165.
- Yamazawa, K., Yagi, Y., and Yachida, M. 1993. Omnidirectional imaging with hyperboloidal projection. In *Proc. IEEE/RISJ International Conference on Intelligent Robots and Systems*, pp. 1029–1034.